Projected spatial reorganization of Köppen–Geiger climate zones under climate change and consequences for population and economic exposure

Dimitri Defrance[a,b*], **Tiffanie Lescure**[b]

[a]The Climate Data Factory, Paris, France
[b]CosmosClimae, Montpellier, France

[*]Corresponding author: dimitri@cosmosclimae.com

Preprint – not peer reviewed

This manuscript is currently under review at *Applied Geography*.

Highlights

Projected spatial reorganization of Köppen–Geiger climate zones under climate change and consequences for population and economic exposure

Dimitri Defrance, Tiffanie Lescure

- Global Köppen–Geiger climate zones are projected to reorganize substantially by the end of the 21st century, with a limited number of dominant transition pathways.
- Transitions from temperate to arid, cold to temperate, and temperate to tropical climates account for the majority of land, population, and GDP exposure under high-emission scenarios.

Projected spatial reorganization of Köppen–Geiger climate zones under climate change and consequences for population and economic exposure

Dimitri Defrance[a,b,*], Tiffanie Lescure[b]

[a] *The Climate Data Factory, Paris, France*
[b] *CosmosClimae, Montpellier, France*

Abstract

Climate change is expected to reorganize macro-climatic regimes at the planetary scale, with implications that extend beyond physical climate variables to the spatial configuration of human systems. While projected shifts in temperature and precipitation are well documented, their translation into categorical climate-regime transitions and associated socio-economic exposure remains insufficiently quantified within a spatial planning perspective.

This study provides a global assessment of projected Köppen–Geiger climate zone transitions and their implications for population and economic exposure by the end of the 21st century. Using bias-corrected CMIP6 projections aggregated at 0.1° resolution and a categorical multi-model ensemble, we map climate-regime changes between 1991–2020 and 2071–2100 under SSP1–2.6, SSP2–4.5, and SSP5–8.5. Gridded population and GDP datasets consistent with the Shared Socioeconomic Pathways are spatially harmonized with the climate classifications to quantify exposure under both fixed baseline and scenario-consistent frameworks.

Results indicate that climate-zone redistribution is spatially structured and dominated by a limited set of directional transitions, notably cold-to-temperate (D→C), temperate-to-arid (C→B), and temperate-to-tropical (C→A) pathways. Under SSP5–8.5, approximately 13.6% of global land surface undergoes a shift in primary climate group by the late 21st century (2071–2100), corresponding to nearly 3.5 billion people and more than 40 trillion USD of economic activity operating within regions experiencing

*dimitri@cosmosclimae.com

a macro-climatic regime transition. Differences across emissions pathways highlight the strong mitigation dependence of large-scale territorial reorganization.

Rather than representing isolated local changes, projected Köppen–Geiger transitions constitute a coherent spatial restructuring of macro-climatic envelopes that intersect directly with patterns of settlement, economic production, and regional development. By linking categorical climate-regime migration with spatially explicit demographic and economic projections, this study provides an operational framework for examining long-term territorial transformation under climate change and supports applied geographical assessments of adaptation and planning under alternative futures.

Keywords: Köppen–Geiger climate zones, Spatial exposure, Population and GDP redistribution, Climate change impacts, Global spatial analysis, Socio-economic vulnerability, Land-surface transitions, Scenario-based assessment, CMIP6

---

1. Introduction

Global demographic and economic trajectories over the 21st century are expected to reshape the spatial distribution of population and wealth under the Shared Socioeconomic Pathways (SSPs) (O'Neill et al., 2014; Riahi et al., 2017). Projections indicate continued concentration of population growth in low- and mid-latitude regions, alongside substantial expansion of economic production in emerging economies (Samir and Lutz, 2017; Wang and Sun, 2022). These development pathways imply that future human systems will not only experience climate change but will do so within a rapidly evolving geography of settlement, infrastructure, and economic activity. Understanding how macro-climatic regimes reorganize relative to these shifting demographic and economic landscapes is therefore central to applied geographical analysis.

Climate change is altering temperature and precipitation patterns worldwide, yet the spatial reorganization of entire macro-climatic regimes remains insufficiently integrated into geographical analysis. While continuous indicators such as mean temperature change (ΔT), precipitation anomalies (ΔP), or frequency of extremes are essential for understanding physical processes, they do not directly describe how the spatial envelopes that structure ecosystems, agriculture, settlement systems, and regional economies are being reorganized. In applied geography and territorial planning, regime boundaries

often matter more than incremental changes in climatic means.

The Köppen–Geiger classification provides a categorical, ecologically grounded framework that integrates temperature and precipitation thresholds into interpretable climate regimes (Köppen, 1936; Peel et al., 2007; Kottek et al., 2006). Unlike single-variable metrics, Köppen classes capture the joint thermal–hydrological structure of climate systems and their historical association with vegetation, land use patterns, and settlement geography. Recent high-resolution updates have enabled consistent global mapping of present and future climate regimes (Beck et al., 2018, 2023).

Previous studies have documented projected shifts in Köppen–Geiger zones under climate change, confirming poleward migration of thermal belts and expansion of arid regimes (Rubel and Kottek, 2010; Rubel et al., 2017; Chan et al., 2020). However, most analyses have remained focused on the physical redistribution of climate types without explicitly quantifying how these transitions intersect with the spatial distribution of population and economic activity.

Parallel research has examined population exposure to climate change using continuous climate indicators. Mora et al. (2017) identified thresholds of deadly heat and projected future human exposure under warming scenarios. Jones et al. (2022) quantified future population exposure to climate extremes under the Shared Socioeconomic Pathways (SSPs), highlighting the combined influence of emissions and demographic trajectories. More recently, Kummu et al. (2023) analysed global population exposure to climate zones in a warming world, demonstrating substantial redistribution across broad climate categories. Importantly, while Kummu et al. (2023) quantify the redistribution of global population across broad climate zones under warming scenarios, their analysis focuses primarily on aggregate exposure shares and does not explicitly characterise the directional structure of climate-regime transitions, nor their intersection with economic geography. In particular, land-surface reallocation between primary climate groups, transition pathway matrices (e.g., C→B, D→C), and the combined evolution of population and GDP within shifting macro-climatic envelopes remain insufficiently examined in an integrated spatial framework. By jointly analysing climate-regime migration, directional transition fluxes, and harmonized projections of both population and economic production, the present study extends exposure assessment toward a territorial restructuring perspective that connects physical climate change with settlement patterns and development trajectories.

These contributions have substantially advanced understanding of climate

exposure, yet important gaps remain. First, most exposure assessments rely on individual climatic variables or extreme-event metrics rather than integrated climatic regimes. Second, analyses are often conducted at coarse spatial resolutions or without explicit quantification of directional transition pathways between climate groups. Third, the joint evolution of land-surface redistribution, demographic concentration, and economic production within shifting macro-climatic envelopes has not been systematically examined within a unified spatial framework.

Recent work in economic and human geography has emphasized the spatial concentration of economic production, infrastructure, and population within specific climatic and environmental corridors (Henderson et al., 2012; Dell et al., 2012). Climate change therefore intersects with pre-existing geographical inequalities rather than operating on a spatially neutral surface. Emerging research on climate–development interactions highlights that future exposure patterns will be shaped not only by climatic shifts, but also by the uneven geography of economic growth, urbanization, and demographic transitions (Byers et al., 2018; Schleussner et al., 2016). Integrating categorical climate-regime migration with spatial economic projections thus provides a framework for examining how macro-climatic restructuring may reinforce or reconfigure existing territorial gradients.

In this study, we address these gaps by integrating bias-corrected CMIP6 projections with categorical Köppen–Geiger classifications and harmonized gridded projections of population and GDP consistent with the SSP framework. We frame climate regime migration as a process of large-scale territorial restructuring that intersects directly with settlement patterns and economic geography.

2. Data and Methods

2.1. Climate data and bias correction

We use bias-corrected and statistically downscaled CMIP6 climate projections processed using the CDFt (Cumulative Distribution Function transform) methodology (Noël et al., 2021; Vrac et al., 2025). The selected global climate models correspond to those commonly employed within the ISIMIP framework, ensuring consistency with established climate-impact modelling standards.

Monthly near-surface air temperature and precipitation were analysed at a spatial resolution of 0.1° over two climatological periods: a historical

reference (1991–2020) and a late 21st-century window (2071–2100). Three emissions scenarios were considered: SSP1–2.6, SSP2–4.5, and SSP5–8.5.

2.2. Köppen–Geiger climate classification

Köppen–Geiger climate classes were derived from monthly climatological means following the standard classification criteria (Peel et al., 2007). The implementation follows the methodological framework described in Defrance et al. (2020). Classifications were computed for the 31 terrestrial Köppen–Geiger classes, excluding ocean grid cells.

For interpretability, detailed classes were aggregated into the five primary climate groups (A–E: Tropical, Arid, Temperate, Cold, Polar). For each model, scenario, and period, classifications were computed independently. A categorical multi-model ensemble was then constructed using a pixel-wise majority vote across models.

2.3. Consistency assessment of the historical classification

Because ERA5-Land served as the observational reference for bias correction, it cannot be considered an independent validation dataset. We therefore assess internal consistency by comparing model-specific Köppen classifications against the ensemble majority classification. This assessment therefore reflects internal consistency with the bias-correction reference rather than an independent out-of-sample validation.

Agreement is quantified using Cohen's Kappa coefficient and overall accuracy at the 31-class and aggregated A–E levels. These validation metrics are reported in the Results section (Table 3).

2.4. Climate zone change detection and transition analysis

Climate regime shifts were identified by comparing ensemble classifications between the historical and future periods at the grid-cell level. A transition is recorded when a grid cell changes Köppen class between periods.

Transitions were analysed at two levels:

(i) detailed 31-class transitions; (ii) aggregated primary group (A–E) transitions.

Directional pathways (e.g., C→B, D→C) were assigned to each grid cell experiencing a change. This directional framing allows explicit identification of dominant transition fluxes structuring global climate-zone redistribution.

2.5. Land surface computation and transition matrices

Grid-cell land areas were computed as a function of latitude and aggregated globally. For each scenario and period, the total land surface associated with each primary climate group was calculated and expressed as a percentage of global terrestrial area.

Directional transition matrices were constructed by cross-tabulating historical versus future primary-group classifications. Matrix entries represent the fraction of total global land transitioning from a historical group (rows) to a future group (columns). Detailed 31-class transition matrices are provided in the Supplementary Material.

2.6. Population data and processing

Gridded population projections were obtained from Wang et al. (2022) and its associated repository (Wang et al., 2024). The dataset provides global 1 km population distributions for 2020–2100 under SSP-consistent demographic trajectories.

Population grids were aggregated to the 0.1° climate analysis grid using area-weighted aggregation and co-registered with the Köppen classifications. Exposure was quantified as the total number of people located within each climate group and expressed as a percentage of global population.

Global population totals differ substantially across SSP narratives (Table 1). SSP2 projects the highest global population by 2100 (9.11 billion), whereas SSP1 and SSP5 exhibit lower late-century totals (6.99 and 7.47 billion, respectively). These demographic contrasts are important for interpreting scenario-specific exposure patterns.

Table 1: Global population under SSP scenarios in 2020 and 2100 (billions).

Scenario	**2020**	**2100**
SSP1	7.56	6.99
SSP2	7.66	9.11
SSP5	7.57	7.47

2.7. GDP data and processing

Gridded GDP data consistent with the SSP narratives were obtained from Wang and Sun (2022) and the associated Zenodo repository (Wang and Sun, 2023). GDP values are expressed in constant 2005 USD.

GDP grids were harmonized to the 0.1° analysis grid and co-registered with the climate classifications. Economic exposure was quantified as the total GDP located within each climate group and expressed as a percentage of global GDP.

Projected global GDP diverges strongly across scenarios (Table 2). While SSP2 reaches 592 trillion USD by 2100, SSP5 exceeds 1000 trillion USD, reflecting sustained high-growth dynamics. SSP1 also exhibits substantial growth but remains below SSP5 levels. These differences condition the magnitude of economic exposure to shifting climate regimes.

Table 2: Global GDP under SSP scenarios (constant 2005 USD, trillion).

Scenario	**2005**	**2100**
SSP1	61.4	646.2
SSP2	61.4	592.2
SSP5	61.4	1075.9

2.8. Socio-economic exposure frameworks

To disentangle climate-driven redistribution from socio-economic development dynamics, two exposure frameworks were implemented:

(1) Fixed baseline framework: Present-day population (2020) and GDP (2005 USD) distributions are overlaid onto future climate classifications. This isolates the effect of climate-zone migration.

(2) Scenario-consistent framework: Future population and GDP projections under each SSP are combined with the corresponding future climate classification, capturing joint climate and socio-economic evolution.

Unless otherwise stated, results focus on SSP5–8.5 as the primary scenario, with SSP1–2.6 and SSP2–4.5 used for sensitivity analysis.

3. Results

3.1. Validation of historical Köppen–Geiger patterns

Figure 1 compares the historical (1991–2020) Köppen–Geiger climate classification derived from ERA5-Land with the categorical multi-model baseline obtained from the five downscaled CMIP6 models using a majority-vote approach. At the full 31-class resolution, large-scale spatial patterns are consistently reproduced, with strong agreement across most continental regions.

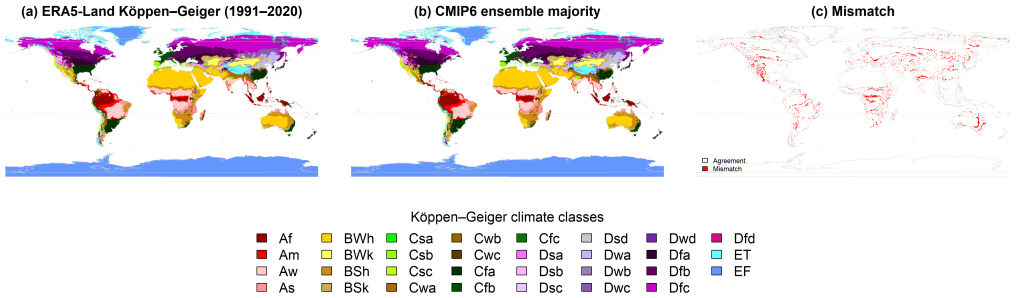

Figure 1: Validation of the Köppen–Geiger baseline classification at 0.1°. (a) Historical (1991–2020) Köppen–Geiger climate classes derived from ERA5-Land. (b) Categorical CMIP6 multi-model ensemble baseline obtained by majority vote across the five downscaled CMIP6 models for the same period. (c) Binary mismatch map highlighting grid cells assigned to different Köppen–Geiger classes between ERA5-Land and the CMIP6 ensemble (red = mismatch; white = agreement). Overall agreement is very high at the full 31-class resolution (Cohen's $\kappa = 0.953$, $P_o = 0.960$), supporting the use of the ensemble classification as a robust baseline for analysing future climate zone transitions.

Spatial mismatches are limited and primarily concentrated in topographically complex areas (e.g. major mountain ranges), coastal transition zones, and semi-arid climate boundaries, where small differences in temperature or precipitation thresholds can lead to class changes.

Quantitative agreement metrics confirm the high consistency between ERA5-Land and the CMIP6 ensemble (Table 3). At the 31-class level, the ensemble exhibits near-perfect agreement with ERA5-Land ($\kappa = 0.953$, $P_o = 0.960$), outperforming all individual models. Agreement further increases when aggregating to the five primary Köppen groups (A–E), with Cohen's Kappa exceeding 0.98, reflecting the greater robustness of broad climate regimes compared to finer subclass distinctions.

Overall, these results demonstrate that the categorical CMIP6 ensemble reliably reproduces observed historical Köppen–Geiger patterns and provides a robust and internally consistent baseline for the analysis of future climate zone transitions and associated socio-economic exposure.

3.2. Projected changes in climate zones

3.2.1. Changes at the full Köppen–Geiger class level

Figure 2 illustrates the projected distribution of Köppen–Geiger climate classes (31 terrestrial classes) for the late 21st century (2071–2100) under the SSP5–8.5 scenario (Figure 2a), together with the corresponding binary

Table 3: Quantitative agreement between ERA5-Land and CMIP6-derived Köppen–Geiger classifications (1991–2020). Agreement is assessed using Cohen's Kappa (κ) and overall accuracy (P_o) at both the full 31-class level and the aggregated Köppen group level (A–E). The multi-model ensemble (majority vote) consistently outperforms individual models.

Target	$\boldsymbol{\kappa_{31}}$	$\boldsymbol{P_{o,31}}$	$\boldsymbol{\kappa_{AE}}$	$\boldsymbol{P_{o,AE}}$
Ensemble majority	0.953	0.960	0.980	0.985
UKESM1-0-LL	0.934	0.944	0.975	0.981
IPSL-CM6A-LR	0.942	0.951	0.977	0.983
MPI-ESM1-2-HR	0.938	0.947	0.975	0.981
GFDL-ESM4	0.942	0.951	0.977	0.983
MRI-ESM2-0	0.944	0.953	0.975	0.982

map of climate-class change relative to the historical baseline (1991–2020) (Figure 2b).

The future classification reveals a large-scale reorganization of detailed climate regimes across all continents. Arid climate classes expand markedly across subtropical regions and continental interiors, including North Africa, the Middle East, Australia, and parts of the Americas, while temperate and cold climate classes undergo extensive spatial redistribution. At high northern latitudes, cold and polar classes retreat poleward, leading to the fragmentation and northward displacement of previously continuous cold-climate belts across Eurasia and North America. Mountainous regions and coastal transition zones display increasingly heterogeneous mosaics of Köppen classes, reflecting the sensitivity of classification thresholds to local gradients in temperature and precipitation.

The binary change map indicates that climate-class transitions affect a substantial fraction of the global land surface by the end of the century, with a strong spatial organization. Transitions are concentrated along latitudinal climate boundaries, at the margins of expanding arid zones, and in regions of complex topography. In contrast, the core of many tropical regions remains comparatively stable at the Köppen class level, despite pronounced changes in underlying climatic variables, highlighting the threshold-based nature of the classification.

Although a wide range of class-to-class transitions occurs at the 31-class level, the spatial structure of change is dominated by coherent regional patterns rather than isolated or random shifts. This motivates the subsequent aggregation of detailed Köppen–Geiger classes into the five primary climate

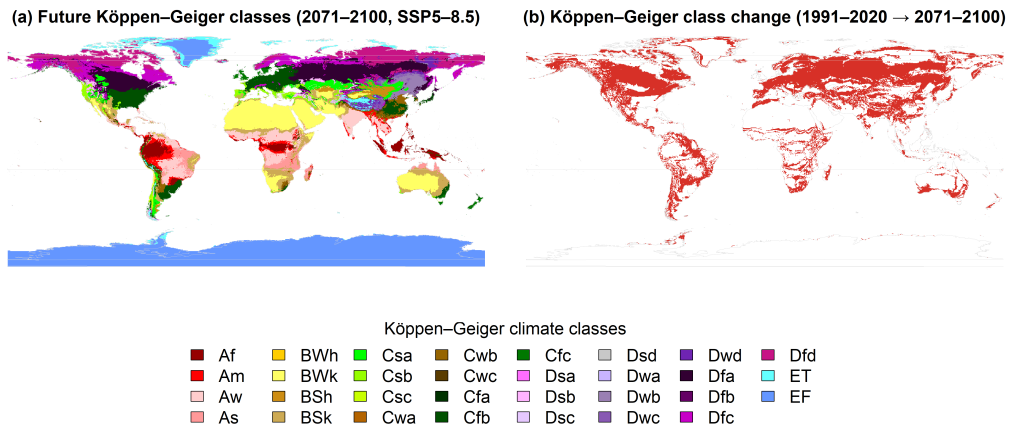

Figure 2: Projected Köppen–Geiger climate classes and transitions under SSP5–8.5 at 0.1°. (a) Multi-model ensemble Köppen–Geiger climate classification for the late 21st century (2071–2100), obtained by majority vote across five downscaled CMIP6 models. (b) Binary map of Köppen–Geiger class change between the historical baseline (1991–2020) and the late-century period, highlighting grid cells experiencing a transition in climate class (red) versus no change (white). The ensemble projection indicates widespread but spatially heterogeneous reorganization of climate regimes, with transitions concentrated in mid-latitude, subtropical, and mountainous regions.

groups (A–E), which provides a more robust and interpretable framework for quantifying changes in land surface area, population exposure, and economic activity.

Equivalent class-level maps and binary change patterns for SSP1–2.6 and SSP2–4.5 are provided in Supplementary Figures S1 and S2, confirming that the spatial organization of regime shifts is consistent across scenarios, albeit with reduced magnitude under lower forcing.

3.2.2. Changes at the primary climate group level (A–E)

To facilitate global interpretation and subsequent socio-economic analyses, results are aggregated into the five primary Köppen–Geiger climate groups (A–E). Figure 3a and Figure 3b show the ensemble classification for the historical and future periods, respectively, while Figure 3c highlights the dominant directional transitions between climate groups for grid cells experiencing a change.

Beyond the overall redistribution of climate regimes, a limited number of transition pathways dominate global spatial patterns. Transitions from

cold to temperate climates (D→C) are widespread across high northern latitudes, particularly in Eurasia and North America, reflecting the systematic poleward retreat and thermal relaxation of cold climate regimes. Polar to cold transitions (E→D) are concentrated along Arctic and Antarctic margins, indicating a contraction of polar conditions towards the highest latitudes.

At lower latitudes, temperate climates act as a major transition hub. Shifts from temperate to arid climates (C→B) are prominent across subtropical regions, including the Mediterranean basin, southern Africa, central Asia, and parts of Australia, consistent with large-scale aridification of transitional climate zones. Transitions from temperate to tropical climates (C→A) occur mainly along the poleward margins of the tropics in South America, Africa, and South and Southeast Asia, reflecting the expansion of tropical climate regimes into formerly temperate areas. Transitions from arid to tropical climates (B→A), although more spatially limited, are observed in selected monsoon-influenced regions and coastal transition zones. The corresponding primary-group maps and dominant transition pathways for SSP1–2.6 and SSP2–4.5 are shown in Supplementary Figures S3 and S4, indicating similar directional structures under lower-emission pathways.

Together, these dominant pathways reveal a structured reorganization of global climate regimes, characterized by poleward shifts of thermal zones and the expansion of warm and dry climates. Spatial agreement across the five individual CMIP6 models for primary climate group classification is illustrated in Supplementary Figure S5. High consensus is observed in core tropical and polar regions, whereas transitional mid-latitude belts exhibit greater inter-model divergence. This spatial structure provides the basis for the subsequent quantification of changes in land surface area, population exposure, and economic activity across primary climate groups.

3.3. Evolution of land surface areas by climate group

Figure 4 synthesizes changes in global land surface associated with the five primary Köppen–Geiger climate groups. Percentages are expressed relative to total global land surface.

Across all future scenarios, arid climates (group B) exhibit a systematic expansion, increasing from approximately 26% of global land area in the historical period (1991–2020) to nearly 28% under SSP5–8.5 (Figure 4a). This expansion is already apparent under SSP1–2.6 and SSP2–4.5, but intensifies monotonically with increasing radiative forcing, indicating a robust large-scale aridification signal.

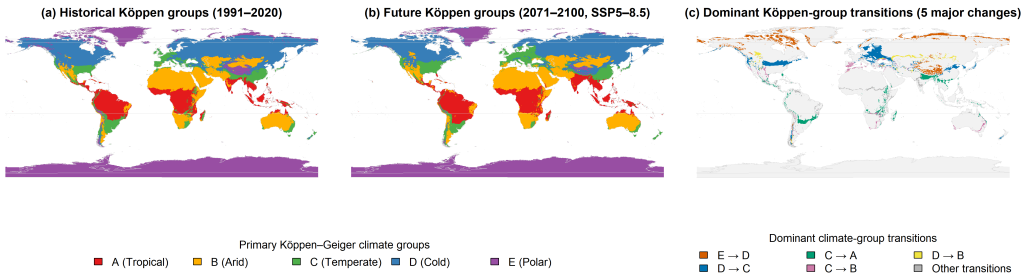

Figure 3: Primary Köppen–Geiger climate groups and dominant transitions under SSP5–8.5 at 0.1°. (a) Historical (1991–2020) distribution of the five primary Köppen–Geiger climate groups (A–E), derived from the categorical CMIP6 multi-model ensemble. (b) Projected distribution of primary Köppen–Geiger climate groups for the late 21st century (2071–2100) under SSP5–8.5. (c) Dominant directional transitions between primary climate groups for grid cells experiencing a change, highlighting the main pathways of climate regime reorganization (e.g. temperate to arid, cold to temperate), while stable regions are masked.

Cold climates (group D) experience the largest net contraction, declining from about 27% of global land surface historically to below 25% under SSP5–8.5. This reduction reflects the widespread poleward retreat of cold climate regimes, particularly across the Northern Hemisphere. Tropical climates (group A) expand more moderately but consistently, increasing from roughly 19.5% to more than 22% of global land area, consistent with a poleward extension of tropical climate conditions. In contrast, temperate climates (group C) show relatively limited net change in total surface area, remaining close to 12–13% globally across scenarios. This apparent stability conceals substantial internal redistribution, as temperate regions act simultaneously as sources and recipients of climate transitions. Polar climates (group E) undergo a clear contraction across all scenarios, with losses accelerating under SSP5–8.5.

The directional structure of these changes is clarified by the transition matrix shown in Figure 4b for SSP5–8.5. While the majority of land surface remains within the same primary climate group, a limited number of asymmetric transition pathways dominate global reorganization. The largest flux corresponds to transitions from cold to temperate climates (D→C), affecting approximately 3.8% of global land surface and reflecting systematic warming across continental interiors. Transitions from polar to cold climates (E→D) account for nearly 2.8% of global land area, highlighting the contraction of

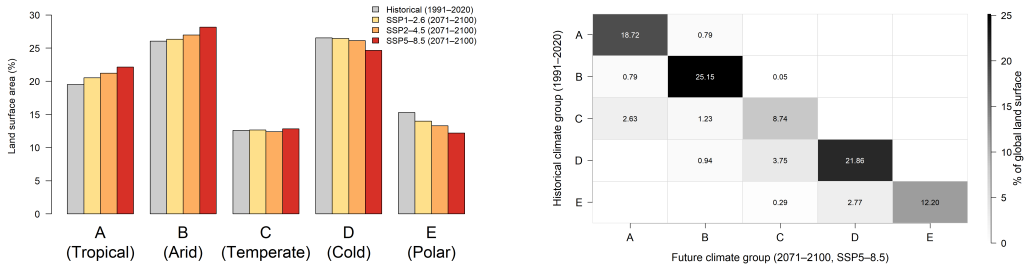

(a) Global land surface area by primary climate group (A–E), expressed as a percentage of total global land surface.

(b) Transition matrix of global land surface between climate groups under SSP5–8.5 (rows: historical; columns: future). Values are % of total global land surface.

Figure 4: Changes in primary Köppen–Geiger climate groups and associated land-surface transitions. (a) Global land surface area by climate group for the historical period (1991–2020) and three future scenarios (2071–2100). (b) Directional transition matrix under SSP5–8.5 quantifying the fraction of global land surface shifting between groups.

polar conditions toward the highest latitudes.

Temperate climates emerge as a central intermediary in the transition network. Transitions from temperate to arid climates (C→B) exceed 1% of global land surface and dominate subtropical regions subject to increasing moisture deficits. Transitions from temperate to tropical climates (C→A), although smaller in magnitude, are spatially coherent along the margins of the tropics and contribute to the expansion of tropical climate regimes. Together, these dominant pathways indicate that global climate-zone shifts are structured and directional rather than diffuse, providing a robust foundation for subsequent analyses of population exposure and economic activity across climate groups.

Under SSP5–8.5, 13.6% of global land surface undergoes a shift in primary Köppen–Geiger climate group by the late 21st century. The full 31-class transition matrix for SSP5–8.5 is provided in Supplementary Figure S6, allowing inspection of detailed subclass-to-subclass reclassifications beyond primary group aggregation. Inter-model variability in total land-surface reclassification is quantified in Supplementary Figure S7. All individual CMIP6 models project large-scale climate-regime shifts under SSP5–8.5, with the fraction of global land surface undergoing a Köppen–Geiger class change ranging between approximately 38% and 52%, while the ensemble majority provides a spatially conservative estimate.

3.4. Population distribution and economic exposure across climate groups

Figure 5 quantifies the redistribution of global population and economic activity across primary Köppen–Geiger climate groups under historical and future conditions. Panels (a) and (b) isolate the effect of climate-zone shifts by holding population (2020) and GDP (2005 USD) constant, respectively. Panels (c) and (d) combine projected climate change with SSP-specific demographic and economic trajectories in 2100.

Under fixed socio-economic baselines (Figures 5a–b), the expansion of arid (B) and tropical (A) climate groups results in a relative increase in the share of global population and GDP located within warmer regimes. Conversely, the contraction of cold (D) and polar (E) climates reduces their relative socio-economic exposure. These shifts intensify with increasing radiative forcing, with the strongest redistribution observed under SSP5–8.5.

When socio-economic change is incorporated (Figures 5c–d), differences between scenarios become more pronounced. Population growth and economic expansion in low- and mid-latitude regions amplify exposure to tropical and arid climates, particularly under SSP2–4.5 and SSP5–8.5. In contrast, high-latitude regions exhibit declining relative shares of both population and GDP within cold climate zones, reflecting both climatic contraction and demographic-economic divergence.

Overall, the results indicate that the socio-economic footprint of climate change is not limited to the physical expansion of climate zones. Rather, projected demographic and economic trajectories substantially modulate the redistribution of exposure across climate regimes, reinforcing the relative concentration of population and GDP in warmer and, in some cases, drier environments. Under the scenario-consistent framework (SSP5 population and GDP in 2100 overlaid on SSP5–8.5 climate classification), this corresponds to 3.5 billion people and >40 trillion USD located in grid cells undergoing a primary-group transition.

3.5. Summary of dominant transition pathways

Across land surface, population, and GDP metrics, global climate-zone reorganization is structured and concentrated along a limited set of directional pathways rather than being diffusely distributed.

At the land-surface level (Figure 4b), the largest transition corresponds to cold-to-temperate shifts (D→C), affecting approximately 3.8% of total

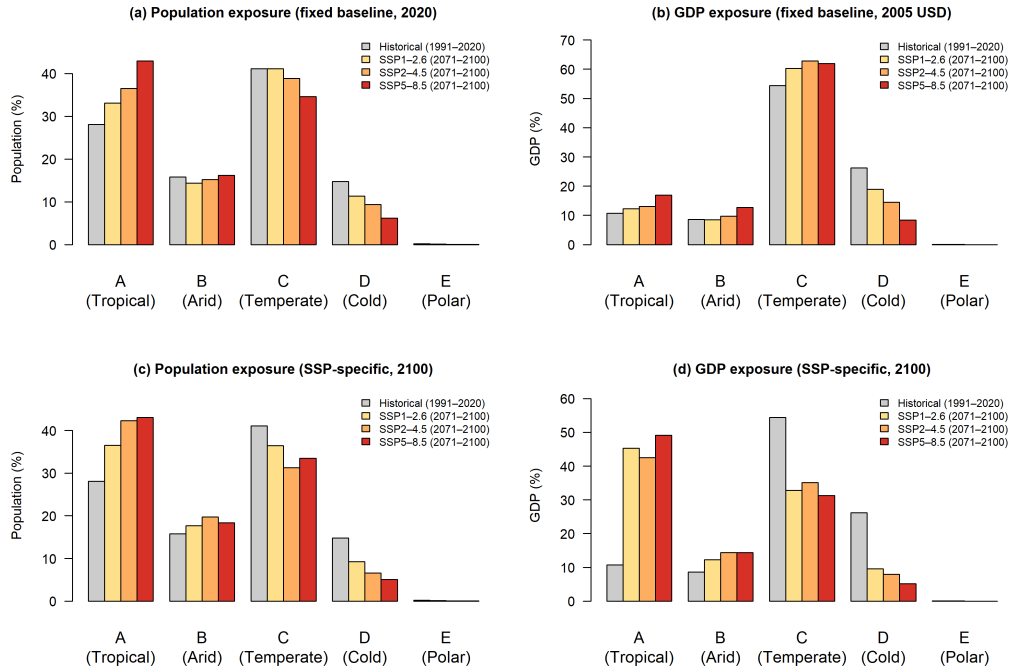

Figure 5: Population and GDP exposure across primary Köppen–Geiger climate groups (A–E). (a) Population exposure assuming fixed baseline population (2020) under historical and future climate classifications. (b) GDP exposure assuming fixed baseline GDP (2005 USD). (c) Population exposure under SSP-specific population projections in 2100. (d) GDP exposure under SSP-specific GDP projections in 2100. Percentages are expressed relative to the total global population or GDP over the common land domain defined by the Köppen classification. Future climate classifications correspond to the 2071–2100 period under SSP1–2.6, SSP2–4.5, and SSP5–8.5.

global land surface under SSP5–8.5. Polar-to-cold transitions (E→D) represent an additional 2.7–2.8% of global land, confirming the systematic poleward retreat of high-latitude climate regimes. Among mid-latitude transitions, temperate-to-arid shifts (C→B) exceed 1% of global land surface and constitute the dominant pathway of subtropical aridification.

When translated into socio-economic exposure (Figure 5), these same pathways structure the redistribution of both population and GDP across climate groups. Under fixed 2020 population, the expansion of tropical (A) and arid (B) groups mechanically increases their share of global population, while the contraction of cold (D) and polar (E) groups reduces theirs. Under

SSP-specific demographic trajectories, this redistribution is further amplified in low- and mid-latitude regions, where projected population growth coincides with expanding tropical and arid climate regimes.

A similar pattern emerges for GDP exposure. Under fixed 2005 GDP, climate-zone redistribution alone shifts economic activity toward warmer regimes. When SSP-consistent GDP projections are considered, economic growth in subtropical and tropical regions reinforces this tendency, particularly under SSP5–8.5.

Importantly, the dominance of C→B, D→C, and C→A transitions is consistent across land surface, population, and GDP metrics, indicating that global climate reorganization follows coherent spatial gradients that intersect directly with the geography of human settlement and economic production.

4. Discussion

4.1. Climate-zone redistribution as large-scale spatial restructuring

Rather than isolated local changes, projected Köppen–Geiger transitions represent a structural reorganization of macro-climatic envelopes at the planetary scale. The dominance of D→C, C→B and C→A pathways reflects systematic poleward displacement of thermal gradients and expansion of subtropical dry regimes. Similar large-scale shifts have been documented in previous Köppen-based assessments (Rubel et al., 2017; Beck et al., 2018; Peel et al., 2007; Chan et al., 2020), yet without explicit integration of socioeconomic exposure.

These transitions redefine the spatial configuration of climate regimes that historically structured agricultural systems, settlement patterns, and regional economic specialization (Peel et al., 2007). By analysing categorical climate zones rather than individual climatic variables, the present study captures the integrated signal of temperature and precipitation change as a coherent geographical restructuring. This perspective is particularly relevant for applied geography, where spatial coherence and regime boundaries often matter more than incremental shifts in climatic means.

Long-run empirical evidence shows that temperature and climate conditions exert persistent effects on economic productivity and growth (Burke et al., 2015; Dell et al., 2012). In this perspective, large-scale shifts in macroclimatic envelopes may alter the spatial economic constraints under which future development unfolds.

4.2. Why directional climate regime transitions matter for spatial planning

Climate regime transitions are not only a matter of aggregate redistribution of climatic conditions, but of directional territorial change that directly affects long-lived socio-spatial systems. The identification of dominant transition pathways (e.g. D→C, C→B, C→A) provides information that is not captured by continuous climate indicators alone and is directly relevant for spatial planning and long-term development strategies.

First, infrastructure systems are inherently path-dependent and climate-specific. Transport networks, energy systems, water infrastructure, and urban form are typically designed based on historical climatic envelopes and expected stationarity over multi-decadal lifetimes (Hallegatte, 2014; Seto et al., 2016). Directional transitions from temperate to arid climates (C→B), for example, imply a structural shift toward higher water stress, altered cooling demand, and increased exposure to heat extremes. When such transitions occur over regions hosting dense infrastructure and growing economic activity, climate regime migration may generate long-term maladaptation risks if planning frameworks remain anchored in historical climate conditions.

Second, agricultural systems are tightly coupled to macro-climatic regimes rather than to isolated climate variables. Crop suitability, phenology, and yield stability depend on the joint thermal and hydrological characteristics captured by Köppen–Geiger classifications (Beck et al., 2018). Directional shifts from temperate to arid (C→B) or temperate to tropical (C→A) regimes imply changes in growing season structure, water availability, and crop viability that extend beyond incremental warming effects. Empirical evidence shows that persistent exposure to warmer or drier climatic conditions can exert long-term constraints on agricultural productivity and rural livelihoods (Lobell et al., 2011; Burke et al., 2015). Identifying where such regime transitions intersect with major agricultural regions therefore provides a spatial diagnostic of potential structural pressure on food systems.

Third, urbanization and population concentration increasingly occur within regions undergoing active climate regime transitions. Many of the dominant C→B and C→A pathways identified in this study affect subtropical and lower mid-latitude regions that simultaneously experience rapid urban growth under SSP2 and SSP5 trajectories. Urban expansion in areas transitioning toward hotter and drier regimes raises specific challenges related to heat stress, water supply, energy demand, and public health (Jones et al., 2022; Mora et al., 2017). Unlike gradual warming signals, categorical regime shifts indicate a qualitative change in the climatic context within which cities develop,

potentially increasing exposure to compound climate stresses if urban form and infrastructure are not adapted accordingly.

Taken together, these examples illustrate that directional climate regime transitions constitute a form of territorial restructuring rather than isolated climatic change. By explicitly identifying where and how macro-climatic envelopes migrate, a directional framework provides actionable spatial information for infrastructure planning, agricultural adaptation, and urban development. Integrating climate regime migration into spatial planning thus complements conventional climate indicators and supports anticipatory decision-making under long-term climate change.

4.3. Socio-economic trajectories and the geography of exposure

A central contribution of this study is the spatial quantification of population and GDP redistribution across climate regimes using harmonized gridded datasets (Wang et al., 2022, 2024; Wang and Sun, 2023, 2022) Results indicate that an increasing share of global population and economic activity is projected to operate within expanding tropical (A) and arid (B) climate groups.

The comparison between fixed socio-economic baselines and SSP-consistent projections demonstrates that climate-zone redistribution alone substantially alters exposure patterns, even in the absence of demographic or economic growth. This reinforces recent findings that spatial exposure to climate change cannot be inferred solely from socio-economic scenarios, but must explicitly account for the geographic displacement of climate regimes themselves (Jones et al., 2022; Kummu et al., 2023).

When SSP-specific demographic trajectories are incorporated, the geographical structure of exposure becomes more pronounced. Under SSP2 and SSP5, sustained population growth in South Asia and Sub-Saharan Africa spatially overlaps with the poleward expansion of tropical climates. This co-location amplifies the relative concentration of global population within warm climate envelopes. In contrast, several high-latitude regions undergoing substantial climatic transitions exhibit slower demographic growth or relative population stabilization under most SSP pathways.

The redistribution of GDP follows a partially distinct logic. While climate-zone shifts mechanically reallocate existing economic activity under fixed baselines, SSP5 in particular projects strong economic growth in several low- and mid-latitude regions. As a result, the share of global GDP operating within tropical and arid climates increases not only because these regimes

expand spatially, but also because economic production intensifies within them. This interaction between climatic migration and economic geography highlights that exposure patterns emerge from the superposition of physical climate change and uneven development dynamics (Riahi et al., 2017). Recent evidence further indicates that climate change has already contributed to widening economic inequality between low- and high-latitude regions (Diffenbaugh and Burke, 2019), suggesting that the redistribution of climate regimes documented here may intersect with pre-existing structural disparities.

Taken together, these results indicate that development trajectories and climate redistribution are spatially intertwined rather than independent processes. The geography of future exposure reflects both the poleward migration of macro-climatic envelopes and the evolving distribution of population and economic activity across continents.

4.4. Latitudinal gradients and North–South configurations

The contraction of cold and polar climates and the expansion of tropical and arid regimes introduce a pronounced latitudinal asymmetry in projected exposure. Model-based assessments indicate that historical warming has reduced economic output in many low-latitude countries while benefiting some high-latitude economies (Callahan and Mankin, 2022), reinforcing the importance of considering latitudinal asymmetries when interpreting projected climate-regime redistribution. While high-latitude regions experience strong climatic transitions, their relative demographic weight declines under several SSPs. Conversely, many low- and mid-latitude regions combine climatic expansion with sustained demographic and economic growth.

Previous studies have documented poleward migration of climate regimes (Rubel et al., 2017; Beck et al., 2018), but without linking these shifts to the geography of economic production and demographic concentration. By integrating SSP-based demographic and economic projections (Riahi et al., 2017; Wang and Sun, 2022; Wang et al., 2022), this study shows that climate regime migration intersects directly with evolving global development corridors. This raises broader geographical questions regarding the climatic contexts within which future economic growth will occur and whether economic activity will increasingly operate within warmer macro-climatic envelopes.

4.5. Methodological considerations and limitations

Several methodological limitations should be acknowledged.

First, the Köppen–Geiger classification is threshold-based and categorical. While this provides interpretability and ecological relevance, it may lead to sensitivity near regime boundaries (Peel et al., 2007). Small variations in temperature or precipitation around classification thresholds can produce class changes that may overemphasize local transitions.

Second, climate projections rely on bias-corrected and statistically downscaled CMIP6 simulations using the CDFt methodology (Noël et al., 2021; Vrac et al., 2025). Although bias correction improves statistical agreement with historical climatology, it does not eliminate structural model uncertainty or potential non-stationarity in climate variability (Herger et al., 2020). Scenario uncertainty further compounds this, as exposure outcomes depend strongly on emissions pathways and socio-economic trajectories (Riahi et al., 2017).

Third, the spatial resolution of 0.1° is appropriate for global and continental-scale analysis but does not capture local-scale topographic gradients, coastal microclimates, or urban heat island effects. Population and GDP exposure are quantified without explicitly modelling migration responses, adaptation strategies, technological innovation, or sectoral restructuring. Consequently, results represent potential redistribution of exposure to shifting climate regimes rather than projections of impacts or vulnerability.

Finally, GDP and population projections under the SSP framework embed substantial uncertainty regarding future demographic and economic development (Riahi et al., 2017). Differences between SSP1–2.6, SSP2–4.5, and SSP5–8.5 in this study illustrate the sensitivity of exposure redistribution to alternative development pathways.

4.6. Exposure versus vulnerability

It is important to emphasize that this analysis quantifies redistribution of exposure to climate regime shifts, not vulnerability or realized impacts. Adaptive capacity, institutional responses, technological change, and migration are not explicitly represented. Climate-induced migration responses, which may significantly reshape future population distributions (Abel et al., 2019; Defrance et al., 2023), are not explicitly represented in the present framework. Identifying where population and economic activity co-locate with shifting climate regimes nonetheless provides a necessary spatial foundation for subsequent risk and adaptation analyses.

4.7. Implications for applied geography

By integrating categorical climate transitions with spatially explicit demographic and economic projections, this study positions Köppen–Geiger classifications as an operational interface between physical climate change and socio-spatial systems. Rather than replacing continuous indicators of warming or precipitation change, the approach complements them by structuring climatic transformation into territorially interpretable regime shifts. The framework is transferable across spatial scales and provides a consistent basis for examining how macro-climatic envelopes intersect with demographic concentration, economic production, and development pathways.

In this perspective, Köppen-based climate regimes function not only as a climatic diagnostic tool but as a spatial lens through which long-term territorial restructuring under climate change can be analysed. Long-lived infrastructure, urban form, and capital investments are typically designed under historical climatic assumptions, generating path dependencies and potential lock-in effects (Seto et al., 2016; Hallegatte, 2014). This interaction between climatic restructuring and infrastructural inertia highlights the importance of anticipatory spatial planning under accelerating climate change. The redistribution of macro-climatic regimes documented here therefore raises strategic questions for infrastructure planning, land-use policy, and regional development strategies, particularly in regions where climatic transitions coincide with rapid population growth and economic expansion.

5. Conclusion

This study provides a global assessment of projected Köppen–Geiger climate zone transitions and their implications for population and economic exposure by the end of the 21st century. Using a categorical multi-model ensemble of bias-corrected CMIP6 projections at 0.1° resolution, we show that climate regime reorganization is structured and dominated by a limited number of directional pathways, notably D→C, C→B, and C→A transitions. These shifts reflect systematic poleward migration of thermal gradients and expansion of subtropical dry regimes, resulting in measurable redistribution of global land surface across primary climate groups. When combined with harmonized gridded projections of population and GDP, these climatic shifts translate into a growing share of global population and economic activity operating within expanding tropical and arid regimes. Climate-zone redistribution alone significantly alters exposure patterns, and socio-economic tra-

jectories under the SSP framework further amplify these dynamics, particularly under high-emission and high-growth pathways. The geography of future exposure therefore emerges from the interaction between physical climate migration and uneven development trajectories, rather than from either process in isolation. Although this analysis does not model vulnerability or adaptation, it provides a spatially explicit diagnostic of where climatic regime change intersects with demographic and economic concentration. Ignoring regime migration risks misaligning long-term infrastructure and development strategies with future climatic envelopes. From a policy perspective, the marked differences between emissions scenarios demonstrate that large-scale redistribution of climatic conditions affecting societies and economies is not inevitable but strongly contingent on mitigation pathways. Köppen–Geiger climate regimes thus offer an operational framework for linking physical climate change with territorial planning, long-term infrastructure strategy, and comparative geographical assessment under alternative futures.

Appendix A. Climate classification under alternative emission scenarios

Figures S1 and S2 present projected Köppen–Geiger class distributions and associated binary change maps under SSP1–2.6 and SSP2–4.5, respectively. While the spatial organization of regime shifts is broadly consistent with SSP5–8.5, the magnitude and spatial continuity of transitions are substantially reduced under lower forcing scenarios.

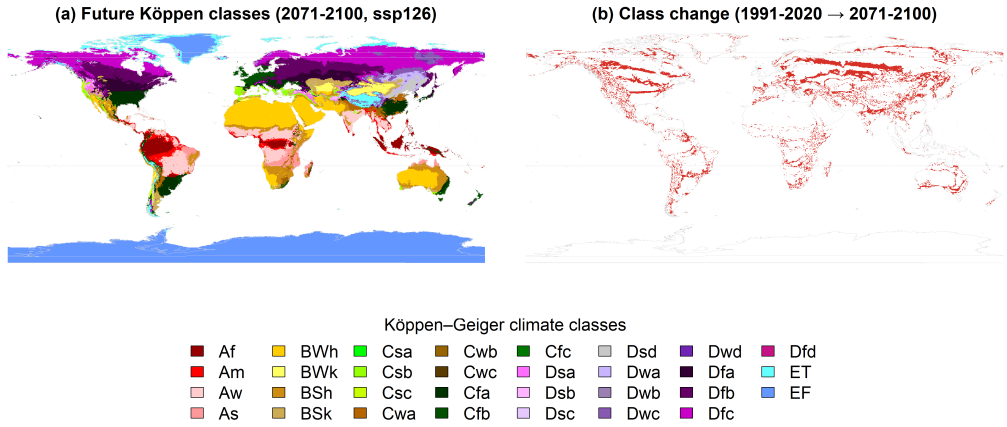

Figure S1: Projected Köppen–Geiger classes and class-level changes under SSP1–2.6 (2071–2100 relative to 1991–2020).

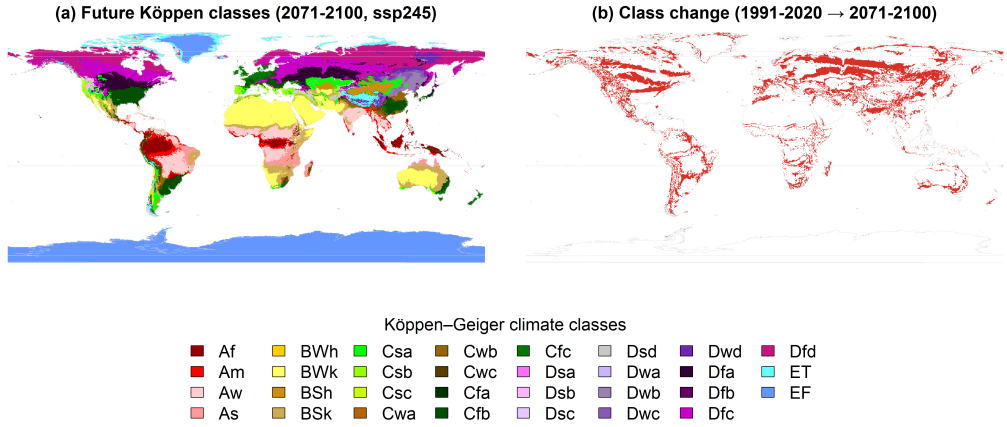

Figure S2: Projected Köppen–Geiger classes and class-level changes under SSP2–4.5 (2071–2100 relative to 1991–2020).

Appendix B. Primary climate group transitions

Figures S3 and S4 show historical and future distributions of primary Köppen–Geiger climate groups (A–E) under SSP1–2.6 and SSP2–4.5, together with dominant directional transitions.

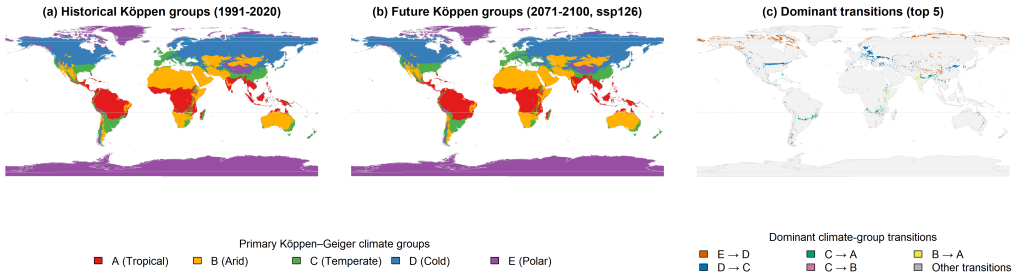

Figure S3: Primary climate groups and dominant transitions under SSP1–2.6.

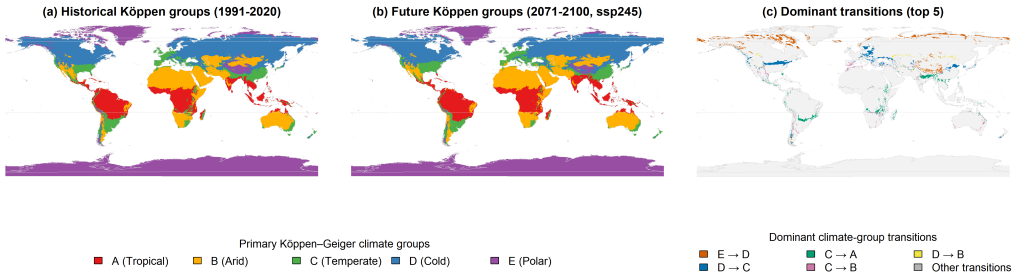

Figure S4: Primary climate groups and dominant transitions under SSP2–4.5.

Appendix C. Ensemble agreement

Figure S5 displays spatial agreement across the five CMIP6 models for primary climate group classifications under SSP5–8.5. Darker areas indicate higher model consensus. High agreement is observed in core tropical and polar regions, while transitional mid-latitude belts exhibit greater inter-model variability.

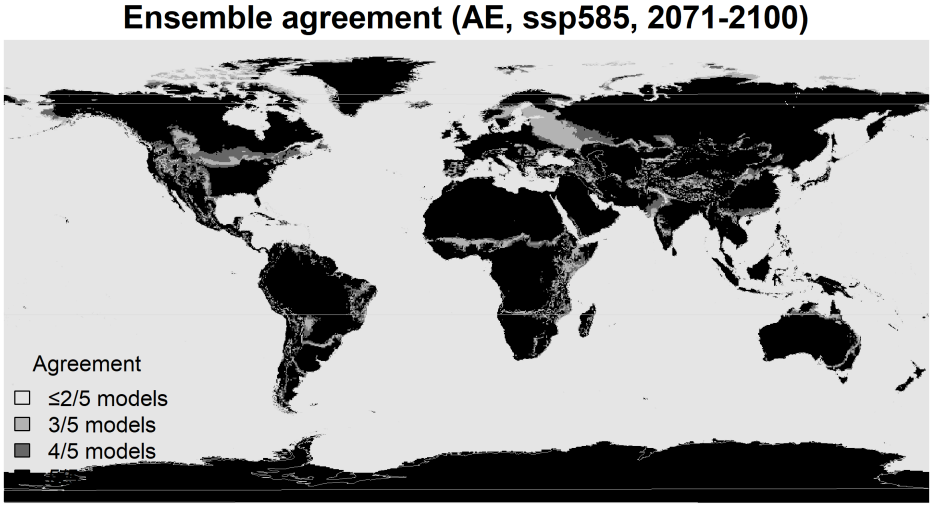

Figure S5: Spatial agreement among five CMIP6 models for primary Köppen–Geiger group classification (2071–2100, SSP5–8.5).

Appendix D. Detailed class-level transition matrix

Figure S6 presents the full 30-class transition matrix under SSP5–8.5, expressed as percentage of total global land surface. Values below 0.05% are not labelled to enhance readability.

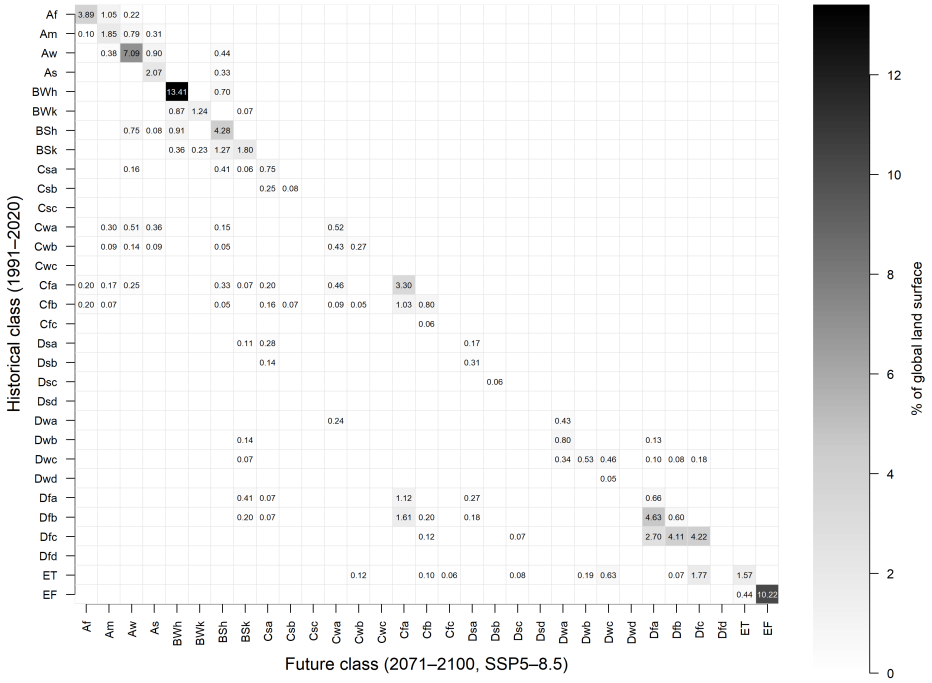

Figure S6: Detailed Köppen–Geiger class transition matrix (1991–2020 to 2071–2100, SSP5–8.5). Values represent percentage of global land surface.

Appendix E. Inter-model spread in land-surface reclassification

Figure S7 quantifies the fraction of global land surface undergoing a Köppen–Geiger class change for each individual CMIP6 model under SSP5–8.5. While all models indicate large-scale regime shifts, the magnitude of reclassification varies between approximately 38% and 52% of global land surface. The ensemble majority classification provides a conservative and spatially robust estimate relative to the most expansive individual projections.

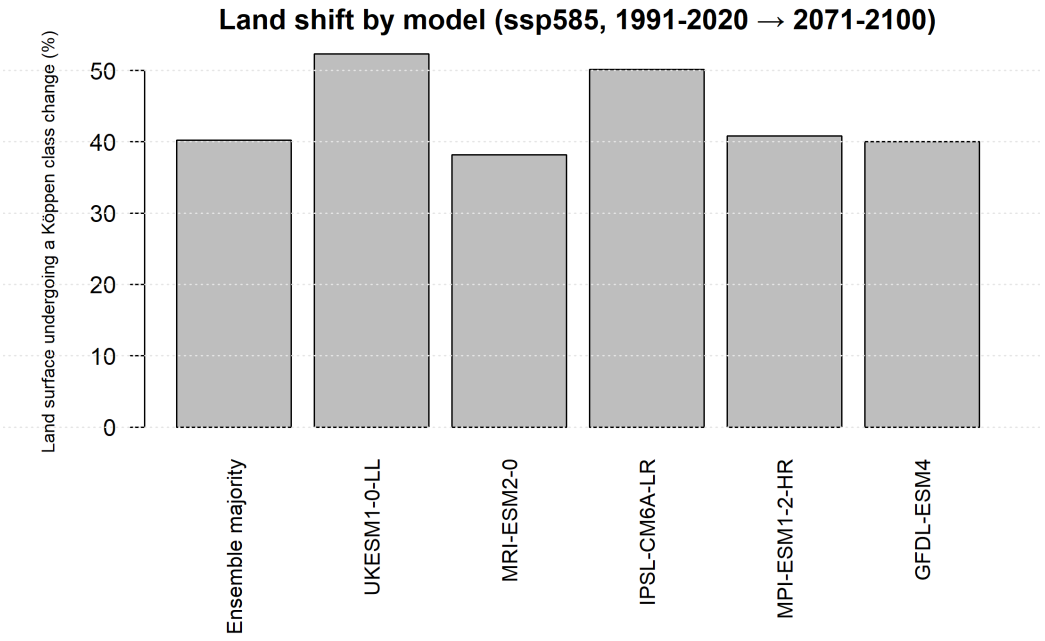

Figure S7: Fraction of global land surface undergoing Köppen–Geiger class change (1991–2020 to 2071–2100, SSP5–8.5) for individual CMIP6 models and the ensemble majority.

Acknowledgements

The climate simulations used in this study were computed using resources of the Institut Pierre-Simon Laplace (IPSL) computing facilities. The author acknowledges the IPSL data infrastructure for providing access to downscaled CMIP6 outputs. ERA5-Land data were obtained through the IPSL TCDF infrastructure and the ESGF node.

Funding

This research received no external funding.

Data availability

Bias-corrected and statistically downscaled CMIP6 climate data were obtained via the IPSL data infrastructure (TCDF) and are accessible for research purposes through the ESGF node (http://esgf-node.ipsl.upmc.fr/ac/subscribe/TCDF/).

ERA5-Land reanalysis data are publicly available through the Copernicus Climate Data Store.

Gridded population projections were obtained from Wang et al. (2022, 2024), and gridded GDP projections from Wang and Sun (2022, 2023), as referenced in the bibliography.

The derived Köppen–Geiger classification maps and transition matrices generated in this study will be made openly available via Zenodo upon publication of the article.

Declaration of competing interest

The authors declare no competing financial or personal interests.

This research was conducted independently within a non-profit association framework and without commercial sponsorship, institutional mandate, or contractual obligation.

CRediT authorship contribution statement

DD: Conceptualization; Methodology; Data curation; Formal analysis; Visualization; Writing – original draft.

TL.: Investigation; Validation; Writing – review & editing.

References

Abel, G.J., Brottrager, M., Crespo Cuaresma, J., Muttarak, R., 2019. Climate, conflict and forced migration. Global Environmental Change 54, 239–249. doi:10.1016/j.gloenvcha.2018.12.003.

Beck, H.E., Wood, E.F., Zimmermann, N.E., et al., 2023. High-resolution cmip6-based köppen–geiger climate projections for the 21st century. Scientific Data 10, 113.

Beck, H.E., Zimmermann, N.E., McVicar, T.R., Vergopolan, N., Berg, A., Wood, E.F., 2018. Present and future köppen–geiger climate classification maps at 1-km resolution. Scientific Data 5, 180214.

Burke, M., Hsiang, S.M., Miguel, E., 2015. Global non-linear effect of temperature on economic production. Nature 527, 235–239. doi:10.1038/nature15725.

Byers, E., Gidden, M., Leclère, D., et al., 2018. Global exposure and vulnerability to multi-sector development and climate change hotspots. Environmental Research Letters 13, 055012.

Callahan, C.W., Mankin, J.S., 2022. National attribution of historical climate damages. Climatic Change 112. doi:10.1007/s10584-022-03387-y.

Chan, D., Wu, Q., Jiang, D., 2020. Global climate regime shifts under warming scenarios. Climate Dynamics 54, 521–540. doi:10.1007/s00382-019-05039-7.

Defrance, D., Delesalle, E., Gubert, F., 2023. Migration response to drought in mali: An analysis using panel data on malian localities over the 1987–2009 period. Environment and Development Economics 28, 171–190. doi:10.1017/S1355770X22000183.

Defrance, D., Ramarohetra, J., Pohl, B., Gallois, M., Vrac, M., 2020. Global and regional climate classification using the köppen–geiger system. Applied Geography 118, 102216. doi:10.1016/j.apgeog.2020.102216.

Dell, M., Jones, B.F., Olken, B.A., 2012. Temperature shocks and economic growth: Evidence from the last half century. American Economic Journal: Macroeconomics 4, 66–95. doi:10.1257/mac.4.3.66.

Diffenbaugh, N.S., Burke, M., 2019. Global warming has increased global economic inequality. Proceedings of the National Academy of Sciences 116, 9808–9813. doi:10.1073/pnas.1816020116.

Hallegatte, S., 2014. Economic Resilience: Definition and Measurement. Policy Research Working Paper 6852. World Bank. URL: https://ssrn.com/abstract=2432352. world Bank Policy Research Working Paper No. 6852.

Henderson, J.V., Storeygard, A., Weil, D.N., 2012. Measuring economic growth from outer space. American Economic Review 102, 994–1028. doi:10.1257/aer.102.2.994.

Herger, N., Abramowitz, G., Whitaker, J., et al., 2020. Bias correction of global climate simulations for hydrological impact studies: Review and evaluation. Earth System Dynamics 11, 753–782.

Jones, B., O'Neill, B.C., McDaniel, L., Tebaldi, C., 2022. Future population exposure to climate extremes under shared socioeconomic pathways. Environmental Research Letters 17, 034023. doi:10.1088/1748-9326/ac4b2b.

Kottek, M., Grieser, J., Beck, C., Rudolf, B., Rubel, F., 2006. World map of the köppen–geiger climate classification updated. Meteorologische Zeitschrift 15, 259–263.

Kummu, M., Taka, M., Guillaume, J.H.A., 2023. Global population exposure to climate zones in a warming world. Nature Communications 14, 349. doi:10.1038/s41467-023-36052-2.

Köppen, W., 1936. Das geographische system der klimate. Handbuch der Klimatologie 1, 1–44.

Lobell, D.B., Schlenker, W., Costa-Roberts, J., 2011. Climate trends and global crop production since 1980. Science 333, 616–620. doi:10.1126/science.1204531, arXiv:https://www.science.org/doi/pdf/10.1126/science.1204531.

Mora, C., Dousset, B., Caldwell, I.R., et al., 2017. Global risk of deadly heat. Nature Climate Change 7, 501–506. doi:10.1038/nclimate3322.

Noël, T., Vrac, M., Levavasseur, G., Servonnat, J., 2021. A trend-preserving bias correction method for climate simulations. Journal of Climate 34, 2629–2648. doi:10.1175/JCLI-D-20-0675.1.

O'Neill, B.C., Kriegler, E., Riahi, K., et al., 2014. A new scenario framework for climate change research: the concept of shared socioeconomic pathways. Climatic Change 122, 387–400. doi:10.1007/s10584-013-0905-2.

Peel, M.C., Finlayson, B.L., McMahon, T.A., 2007. Updated world map of the köppen–geiger climate classification. Hydrology and Earth System Sciences 11, 1633–1644.

Riahi, K., van Vuuren, D.P., Kriegler, E., et al., 2017. The shared socioeconomic pathways and their energy, land use, and greenhouse gas emissions implications. Global Environmental Change 42, 153–168. doi:10.1016/j.gloenvcha.2016.05.009.

Rubel, F., Brugger, K., Haslinger, K., Auer, I., 2017. Observed and projected climate shifts 1901–2100 depicted by world maps of the köppen–geiger climate classification. Meteorologische Zeitschrift 26, 115–125. doi:10.1127/metz/2016/0816.

Rubel, F., Kottek, M., 2010. Observed and projected climate shifts 1901–2100 depicted by world maps of the köppen-geiger climate classification. Meteorologische Zeitschrift 19, 135–141.

Samir, K.C., Lutz, W., 2017. The human core of the shared socioeconomic pathways: Population scenarios by age, sex and level of education. Global Environmental Change 42, 181–192. doi:10.1016/j.gloenvcha.2014.06.004.

Schleussner, C.F., Lissner, T.K., Fischer, E.M., et al., 2016. Differential climate impacts for policy-relevant limits to global warming: the case of 1.5 °c and 2 °c. Earth System Dynamics 7, 327–351.

Seto, K.C., Davis, S.J., Mitchell, R.B., Stokes, E.C., Unruh, G., Ürge Vorsatz, D., 2016. Carbon lock-in: Types, causes, and policy implications. Annual Review of Environment and Resources 41, 425–452. doi:10.1146/annurev-environ-110615-085934.

Vrac, M., Loukos, H., Noël, T., Defrance, D., 2025. Bias correction of climate simulations using CDFt: recent advances and perspectives. Climate Dynamics In press.

Wang, T., Sun, F., 2022. Global gridded gdp data set consistent with the shared socioeconomic pathways. Scientific Data 9, 221. doi:10.1038/s41597-022-01300-x.

Wang, T., Sun, F., 2023. Global gridded GDP under the historical and future scenarios. doi:10.5281/zenodo.7898409.

Wang, X., Meng, X., Long, Y., 2022. Projecting 1 km-grid population distributions from 2020 to 2100 globally under shared socioeconomic pathways. Scientific Data 9, 563. doi:10.1038/s41597-022-01675-x.

Wang, X., Meng, X., Long, Y., 2024. Projecting 1 km-grid population distributions from 2020 to 2100 globally under shared socioeconomic pathways. doi:10.6084/m9.figshare.19608594.v3.